

Search for Baryonic Decays of $\psi(3770)$ and $\psi(4040)$

M. Ablikim¹, M. N. Achasov^{6,a}, O. Albayrak³, D. J. Ambrose³⁹, F. F. An¹, Q. An⁴⁰, J. Z. Bai¹, R. Baldini Ferroli^{17A}, Y. Ban²⁶, J. Becker², J. V. Bennett¹⁶, M. Bertani^{17A}, J. M. Bian³⁸, E. Boger^{19,b}, O. Bondarenko²⁰, I. Boyko¹⁹, R. A. Briere³, V. Bytev¹⁹, H. Cai⁴⁴, X. Cai¹, O. Cakir^{34A}, A. Calcaterra^{17A}, G. F. Cao¹, S. A. Cetin^{34B}, J. F. Chang¹, G. Chelkov^{19,b}, G. Chen¹, H. S. Chen¹, J. C. Chen¹, M. L. Chen¹, S. J. Chen²⁴, X. Chen²⁶, Y. B. Chen¹, H. P. Cheng¹⁴, Y. P. Chu¹, D. Cronin-Hennessy³⁸, H. L. Dai¹, J. P. Dai¹, D. Dedovich¹⁹, Z. Y. Deng¹, A. Denig¹⁸, I. Denysenko¹⁹, M. Destefanis^{43A,43C}, W. M. Ding²⁸, Y. Ding²², L. Y. Dong¹, M. Y. Dong¹, S. X. Du⁴⁶, J. Fang¹, S. S. Fang¹, L. Fava^{43B,43C}, C. Q. Feng⁴⁰, P. Friedel², C. D. Fu¹, J. L. Fu²⁴, O. Fuks^{19,b}, Y. Gao³³, C. Geng⁴⁰, K. Goetzen⁷, W. X. Gong¹, W. Gradl¹⁸, M. Greco^{43A,43C}, M. H. Gu¹, Y. T. Gu⁹, Y. H. Guan³⁶, A. Q. Guo²⁵, L. B. Guo²³, T. Guo²³, Y. P. Guo²⁵, Y. L. Han¹, F. A. Harris³⁷, K. L. He¹, M. He¹, Z. Y. He²⁵, T. Held², Y. K. Heng¹, Z. L. Hou¹, C. Hu²³, H. M. Hu¹, J. F. Hu³⁵, T. Hu¹, G. M. Huang⁴, G. S. Huang⁴⁰, J. S. Huang¹², L. Huang¹, X. T. Huang²⁸, Y. Huang²⁴, Y. P. Huang¹, T. Hussain⁴², C. S. Ji⁴⁰, Q. Ji¹, Q. P. Ji²⁵, X. B. Ji¹, X. L. Ji¹, L. L. Jiang¹, X. S. Jiang¹, J. B. Jiao²⁸, Z. Jiao¹⁴, D. P. Jin¹, S. Jin¹, F. F. Jing³³, N. Kalantar-Nayestanaki²⁰, M. Kavatsyuk²⁰, B. Kopf², M. Kornicer³⁷, W. Kuehn³⁵, W. Lai¹, J. S. Lange³⁵, P. Larin¹¹, M. Leyhe², C. H. Li¹, Cheng Li⁴⁰, Cui Li⁴⁰, D. M. Li⁴⁶, F. Li¹, G. Li¹, H. B. Li¹, J. C. Li¹, K. Li¹⁰, Lei Li¹, Q. J. Li¹, S. L. Li¹, W. D. Li¹, W. G. Li¹, X. L. Li²⁸, X. N. Li¹, X. Q. Li²⁵, X. R. Li²⁷, Z. B. Li³², H. Liang⁴⁰, Y. F. Liang³⁰, Y. T. Liang³⁵, G. R. Liao³³, X. T. Liao¹, D. Lin¹¹, B. J. Liu¹, C. L. Liu³, C. X. Liu¹, F. H. Liu²⁹, Fang Liu¹, Feng Liu⁴, H. Liu¹, H. B. Liu⁹, H. H. Liu¹³, H. M. Liu¹, H. W. Liu¹, J. P. Liu⁴⁴, K. Liu³³, K. Y. Liu²², P. L. Liu²⁸, Q. Liu³⁶, S. B. Liu⁴⁰, X. Liu²¹, Y. B. Liu²⁵, Z. A. Liu¹, Zhiqiang Liu¹, Zhiqing Liu¹, H. Loehner²⁰, X. C. Lou^{1,c}, G. R. Lu¹², H. J. Lu¹⁴, J. G. Lu¹, Q. W. Lu²⁹, X. R. Lu³⁶, Y. P. Lu¹, C. L. Luo²³, M. X. Luo⁴⁵, T. Luo³⁷, X. L. Luo¹, M. Lv¹, C. L. Ma³⁶, F. C. Ma²², H. L. Ma¹, Q. M. Ma¹, S. Ma¹, T. Ma¹, X. Y. Ma¹, F. E. Maas¹¹, M. Maggiora^{43A,43C}, Q. A. Malik⁴², Y. J. Mao²⁶, Z. P. Mao¹, J. G. Messchendorp²⁰, J. Min¹, T. J. Min¹, R. E. Mitchell¹⁶, X. H. Mo¹, H. Moeini²⁰, C. Morales Morales¹¹, K. Moriya¹⁶, N. Yu. Muchnoi^{6,a}, H. Muramatsu³⁹, Y. Nefedov¹⁹, C. Nicholson³⁶, I. B. Nikolaev^{6,a}, Z. Ning¹, S. L. Olsen²⁷, Q. Ouyang¹, S. Pacetti^{17B}, M. Pelizaeus², H. P. Peng⁴⁰, K. Peters⁷, J. L. Ping²³, R. G. Ping¹, R. Poling³⁸, E. Prencipe¹⁸, M. Qi²⁴, S. Qian¹, C. F. Qiao³⁶, L. Q. Qin²⁸, X. S. Qin¹, Y. Qin²⁶, Z. H. Qin¹, J. F. Qiu¹, K. H. Rashid⁴², G. Rong¹, X. D. Ruan⁹, A. Sarantsev^{19,d}, B. D. Schaefer¹⁶, M. Shao⁴⁰, C. P. Shen^{37,e}, X. Y. Shen¹, H. Y. Sheng¹, K. H. Shepherd¹⁶, W. M. Song¹, X. Y. Song¹, S. Spataro^{43A,43C}, B. Spruck³⁵, D. H. Sun¹, G. X. Sun¹, J. F. Sun¹², S. S. Sun¹, Y. J. Sun⁴⁰, Y. Z. Sun¹, Z. J. Sun¹, Z. T. Sun⁴⁰, C. J. Tang³⁰, X. Tang¹, I. Tapan^{34C}, E. H. Thorndike³⁹, D. Toth³⁸, M. Ullrich³⁵, I. Uman^{34B}, G. S. Varner³⁷, B. Q. Wang²⁶, D. Wang²⁶, D. Y. Wang²⁶, K. Wang¹, L. L. Wang¹, L. S. Wang¹, M. Wang²⁸, P. Wang¹, P. L. Wang¹, Q. J. Wang¹, S. G. Wang²⁶, X. F. Wang³³, X. L. Wang⁴⁰, Y. D. Wang^{17A}, Y. F. Wang¹, Y. Q. Wang¹⁸, Z. Wang¹, Z. G. Wang¹, Z. Y. Wang¹, D. H. Wei⁸, J. B. Wei²⁶, P. Weidenkaff¹⁸, Q. G. Wen⁴⁰, S. P. Wen¹, M. Werner³⁵, U. Wiedner², L. H. Wu¹, N. Wu¹, S. X. Wu⁴⁰, W. Wu²⁵, Z. Wu¹, L. G. Xia³³, Y. X. Xia¹⁵, Z. J. Xiao²³, Y. G. Xie¹, Q. L. Xiu¹, G. F. Xu¹, G. M. Xu²⁶, Q. J. Xu¹⁰, Q. N. Xu³⁶, X. P. Xu^{31,27}, Z. R. Xu⁴⁰, F. Xue⁴, Z. Xue¹, L. Yan⁴⁰, W. B. Yan⁴⁰, Y. H. Yan¹⁵, H. X. Yang¹, Y. Yang⁴, Y. X. Yang⁸, H. Ye¹, M. Ye⁵, B. X. Yu¹, C. X. Yu²⁵, H. W. Yu²⁶, J. S. Yu²¹, S. P. Yu²⁸, C. Z. Yuan¹, Y. Yuan¹, A. A. Zafar⁴², A. Zallo^{17A}, S. L. Zang²⁴, Y. Zeng¹⁵, B. X. Zhang¹, B. Y. Zhang¹, C. Zhang²⁴, C. C. Zhang¹, D. H. Zhang¹, H. H. Zhang³², H. Y. Zhang¹, J. Q. Zhang¹, J. W. Zhang¹, J. Y. Zhang¹, J. Z. Zhang¹, LiLi Zhang¹⁵, R. Zhang³⁶, S. H. Zhang¹, X. J. Zhang¹, X. Y. Zhang²⁸, Y. Zhang¹, Y. H. Zhang¹, Z. P. Zhang⁴⁰, Z. Y. Zhang⁴⁴, Zhenghao Zhang⁴, G. Zhao¹, H. S. Zhao¹, J. W. Zhao¹, K. X. Zhao²³, Lei Zhao⁴⁰, Ling Zhao¹, M. G. Zhao²⁵, Q. Zhao¹, S. J. Zhao⁴⁶, T. C. Zhao¹, X. H. Zhao²⁴, Y. B. Zhao¹, Z. G. Zhao⁴⁰, A. Zhemchugov^{19,b}, B. Zheng⁴¹, J. P. Zheng¹, Y. H. Zheng³⁶, B. Zhong²³, L. Zhou¹, X. Zhou⁴⁴, X. K. Zhou³⁶, X. R. Zhou⁴⁰, C. Zhu¹, K. Zhu¹, K. J. Zhu¹, S. H. Zhu¹, X. L. Zhu³³, Y. C. Zhu⁴⁰, Y. M. Zhu²⁵, Y. S. Zhu¹, Z. A. Zhu¹, J. Zhuang¹, B. S. Zou¹, J. H. Zou¹

(BESIII Collaboration)

¹ Institute of High Energy Physics, Beijing 100049, People's Republic of China

² Bochum Ruhr-University, D-44780 Bochum, Germany

³ Carnegie Mellon University, Pittsburgh, Pennsylvania 15213, USA

⁴ Central China Normal University, Wuhan 430079, People's Republic of China

⁵ China Center of Advanced Science and Technology, Beijing 100190, People's Republic of China

⁶ G.I. Budker Institute of Nuclear Physics SB RAS (BINP), Novosibirsk 630090, Russia

⁷ GSI Helmholtzcentre for Heavy Ion Research GmbH, D-64291 Darmstadt, Germany

⁸ Guangxi Normal University, Guilin 541004, People's Republic of China

⁹ GuangXi University, Nanning 530004, People's Republic of China

¹⁰ Hangzhou Normal University, Hangzhou 310036, People's Republic of China

¹¹ Helmholtz Institute Mainz, Johann-Joachim-Becher-Weg 45, D-55099 Mainz, Germany

¹² Henan Normal University, Xinxiang 453007, People's Republic of China

¹³ Henan University of Science and Technology, Luoyang 471003, People's Republic of China

¹⁴ Huangshan College, Huangshan 245000, People's Republic of China

¹⁵ Hunan University, Changsha 410082, People's Republic of China

¹⁶ Indiana University, Bloomington, Indiana 47405, USA

¹⁷ (A)INFN Laboratori Nazionali di Frascati, I-00044, Frascati,

Italy; (B)INFN and University of Perugia, I-06100, Perugia, Italy

¹⁸ Johannes Gutenberg University of Mainz, Johann-Joachim-Becher-Weg 45, D-55099 Mainz, Germany

¹⁹ Joint Institute for Nuclear Research, 141980 Dubna, Moscow region, Russia

- ²⁰ *KVI, University of Groningen, NL-9747 AA Groningen, The Netherlands*
²¹ *Lanzhou University, Lanzhou 730000, People's Republic of China*
²² *Liaoning University, Shenyang 110036, People's Republic of China*
²³ *Nanjing Normal University, Nanjing 210023, People's Republic of China*
²⁴ *Nanjing University, Nanjing 210093, People's Republic of China*
²⁵ *Nankai University, Tianjin 300071, People's Republic of China*
²⁶ *Peking University, Beijing 100871, People's Republic of China*
²⁷ *Seoul National University, Seoul, 151-747 Korea*
²⁸ *Shandong University, Jinan 250100, People's Republic of China*
²⁹ *Shanxi University, Taiyuan 030006, People's Republic of China*
³⁰ *Sichuan University, Chengdu 610064, People's Republic of China*
³¹ *Soochow University, Suzhou 215006, People's Republic of China*
³² *Sun Yat-Sen University, Guangzhou 510275, People's Republic of China*
³³ *Tsinghua University, Beijing 100084, People's Republic of China*
³⁴ (A) *Ankara University, Dogol Caddesi, 06100 Tandogan, Ankara, Turkey*; (B) *Dogus University, 34722 Istanbul, Turkey*; (C) *Uludag University, 16059 Bursa, Turkey*
³⁵ *Universitaet Giessen, D-35392 Giessen, Germany*
³⁶ *University of Chinese Academy of Sciences, Beijing 100049, People's Republic of China*
³⁷ *University of Hawaii, Honolulu, Hawaii 96822, USA*
³⁸ *University of Minnesota, Minneapolis, Minnesota 55455, USA*
³⁹ *University of Rochester, Rochester, New York 14627, USA*
⁴⁰ *University of Science and Technology of China, Hefei 230026, People's Republic of China*
⁴¹ *University of South China, Hengyang 421001, People's Republic of China*
⁴² *University of the Punjab, Lahore-54590, Pakistan*
⁴³ (A) *University of Turin, I-10125, Turin, Italy*; (B) *University of Eastern Piedmont, I-15121, Alessandria, Italy*; (C) *INFN, I-10125, Turin, Italy*
⁴⁴ *Wuhan University, Wuhan 430072, People's Republic of China*
⁴⁵ *Zhejiang University, Hangzhou 310027, People's Republic of China*
⁴⁶ *Zhengzhou University, Zhengzhou 450001, People's Republic of China*
- ^a *Also at the Novosibirsk State University, Novosibirsk, 630090, Russia*
^b *Also at the Moscow Institute of Physics and Technology, Moscow 141700, Russia*
^c *Also at University of Texas at Dallas, Richardson, Texas 75083, USA*
^d *Also at the PNPI, Gatchina 188300, Russia*
^e *Present address: Nagoya University, Nagoya 464-8601, Japan*

By analyzing data samples of 2.9 fb^{-1} collected at $\sqrt{s} = 3.773 \text{ GeV}$, 482 pb^{-1} collected at $\sqrt{s} = 4.009 \text{ GeV}$ and 67 pb^{-1} collected at $\sqrt{s} = 3.542, 3.554, 3.561, 3.600$ and 3.650 GeV with the BESIII detector at the BEPCII storage ring, we search for $\psi(3770)$ and $\psi(4040)$ decay to baryonic final states, including $\Lambda\bar{\Lambda}\pi^+\pi^-$, $\Lambda\bar{\Lambda}\pi^0$, $\Lambda\bar{\Lambda}\eta$, $\Sigma^+\bar{\Sigma}^-$, $\Sigma^0\bar{\Sigma}^0$, $\Xi^-\bar{\Xi}^+$ and $\Xi^0\bar{\Xi}^0$ decays. None are observed, and upper limits are set at the 90% confidence level.

PACS numbers: 13.25.Gv, 12.38.Qk, 14.40.Gx

I. INTRODUCTION

Above $D\bar{D}$ threshold, there are several broad $c\bar{c}$ resonance peaks, namely $\psi(3770)$, $\psi(4040)$, $\psi(4160)$ and $\psi(4415)$. It is important to study the properties of these excited $J^{PC} = 1^{--}$ charmonium states. The $\psi(3770)$ and $\psi(4040)$ resonances decay quite abundantly into open-charm final states. While charmless decays of the $\psi(3770)$ and $\psi(4040)$ are possible, their branching fractions are supposed to be highly suppressed.

Unexpectedly, the BES Collaboration measured the branching fraction for $\psi(3770)$ decay to non- $D\bar{D}$ to be $(15 \pm 5)\%$ by utilizing varied methods [1–4] under the hypothesis that only one simple $\psi(3770)$ resonance exists in the center-of-mass energy region from 3.70 to 3.87 GeV. Meanwhile, the CLEO Collaboration obtained the branching fraction $\mathcal{B}(\psi(3770) \rightarrow \text{non-}D\bar{D}) = (-3.3 \pm$

$1.4_{-4.8}^{+6.6})\%$, which corresponds to $\mathcal{B}(\psi(3770) \rightarrow \text{non-}D\bar{D}) < 9\%$ at the 90% Confidence Level (C.L.) when considering only physical (positive) values [5]. The results are obtained under the assumption that the interference of the resonance decay, $\psi(3686) \rightarrow \gamma^* \rightarrow q\bar{q} \rightarrow \text{hadrons}$ with the continuum annihilation, $\gamma^* \rightarrow q\bar{q} \rightarrow \text{hadrons}$, is destructive at $\sqrt{s} = 3.671 \text{ GeV}$ and constructive at $\sqrt{s} = 3.773 \text{ GeV}$ [6]. Since a large non- $D\bar{D}$ component conflicts with the theoretical prediction [7, 8], it is important to identify the non- $D\bar{D}$ decays of the $\psi(3770)$, which will place the large non- $D\bar{D}$ component on a solid footing and shed light on the nature of the $\psi(3770)$.

The BES Collaboration observed the first non- $D\bar{D}$ decay, $\psi(3770) \rightarrow \pi^+\pi^-J/\psi$, with a branching fraction of $(0.34 \pm 0.14 \pm 0.09)\%$ [9]. The CLEO Collaboration confirmed the same hadronic transition [10], and observed other hadronic transitions $\pi^0\pi^0J/\psi$, $\eta J/\psi$ [10], and ra-

diative transitions $\gamma\chi_{cJ}(J = 0, 1)$ [11, 12] to lower-lying charmonium states, and the decay to light hadrons $\phi\eta$ [13]. While BES and CLEO have continued to search for exclusive non- $D\bar{D}$ decays of $\psi(3770)$, the total non- $D\bar{D}$ exclusive components are less than 2% [14], which motivates the search for other exclusive non- $D\bar{D}$ final states.

The $\psi(4040)$ is generally considered to be the 3^3S_1 charmonium state. Studies of its charmless decays are also interesting, and there are fewer experimental measurements of the branching fractions for $\psi(4040)$ decay. The BESIII Collaboration observed the first production of $e^+e^- \rightarrow \eta J/\psi$ at $\sqrt{s} = 4.009$ GeV. Assuming the $\eta J/\psi$ signal is from a hadronic transition of the $\psi(4040)$, the fractional transition rate is determined to be $\mathcal{B}(\psi(4040) \rightarrow \eta J/\psi) = (5.2 \pm 0.5 \pm 0.2 \pm 0.5) \times 10^{-3}$ [15]. Searching for other exclusive non- $D\bar{D}$ decays of $\psi(4040)$ is also urgently needed.

Since D mesons are not sufficiently massive to decay to baryon pairs, modes with baryons would be unambiguous evidence for non- $D\bar{D}$ decays of $\psi(3770)$. Further, no searches for baryonic decays of $\psi(4040)$ exist. In this article, we report results of searches for baryonic decays of $\psi(3770)$ and $\psi(4040)$, including final states with baryon pairs ($\Sigma^+\bar{\Sigma}^-$, $\Sigma^0\bar{\Sigma}^0$, $\Xi^-\bar{\Xi}^+$, $\Xi^0\bar{\Xi}^0$) and other $B\bar{B}X$ modes ($\Lambda\bar{\Lambda}\pi^+\pi^-$, $\Lambda\bar{\Lambda}\pi^0$, $\Lambda\bar{\Lambda}\eta$).

II. EXPERIMENT AND DATA SAMPLES

The data samples used in this analysis were collected at the $\psi(3770)$ resonance ($\sqrt{s} = 3.773$ GeV), the $\psi(4040)$ resonance ($\sqrt{s} = 4.009$ GeV) and the surrounding continuum ($\sqrt{s} = 3.542, 3.554, 3.561, 3.600$ and 3.650 GeV), in e^+e^- collisions produced by the Beijing Electron Positron Collider II (BEPCII) and acquired with the BESIII detector. BESIII/BEPCII [16] is the major upgrade of BESII/BEPC [17] for study of hadron spectroscopy and τ -charm physics [18]. BEPCII is a double-ring e^+e^- collider designed for a peak luminosity of 10^{33} $\text{cm}^{-2}\text{s}^{-1}$ at a beam current of 0.93 A at the $\psi(3770)$ peak. The BESIII detector with a solid angle coverage of 93% of 4π consists of the following components: (1) A small cell, helium-based main drift chamber (MDC) with 43 layers, providing an average single wire resolution of $135 \mu\text{m}$, a dE/dx resolution that is better than 6%, and a momentum resolution of 0.5% for 1 GeV/ c charged particles in the 1.0 Tesla magnetic field; (2) An Electro-Magnetic Calorimeter (EMC) consisting of 6240 CsI(Tl) crystals arranged in a cylindrical structure (barrel) and two end caps. The energy resolution for photons with an energy of 1.0 GeV is 2.5% (5.0%) in the barrel (end caps), and the position resolution is 6 mm (9 mm) in the barrel (end caps); (3) A Time-of-Flight (TOF) system for particle identification (PID) composed of two layers (one layer) of scintillator with time resolution of 80 ps (110 ps) in the barrel (end caps), corresponding to a K/π separation by more than 2σ for momenta below

about 1 GeV/ c ; (4) These components are all enclosed in a superconducting solenoidal magnet providing a 1.0 Tesla magnetic field. (5) A muon chamber system (MUC) consisting of 1000 m^2 of resistive plate chambers (RPC) arranged in 9 layers in the barrel and 8 layers in the end caps with spatial resolution of 2 cm.

The integrated luminosity (\mathcal{L}) of the data sets is measured by using large angle bhabha scatter events. The data sets for this analysis consist of $\mathcal{L} = 2.9 \text{ fb}^{-1}$ of e^+e^- annihilation data collected at the center-of-mass energy of 3.773 GeV, the peak of the $\psi(3770)$ resonance, 482 pb^{-1} data taken at the center-of-mass energy of 4.009 GeV, near the peak of the $\psi(4040)$ resonance and continuum data, which is used to determine the non-resonant continuum background subtraction, consisting of 23 pb^{-1} taken at center-of-mass energies of 3.542, 3.554, 3.561, 3.600 GeV and 44 pb^{-1} taken at the center-of-mass energy of 3.650 GeV.

The evaluation of detection efficiency, the optimization of the event selection and the estimation of physics backgrounds are achieved with simulated Monte Carlo (MC) samples. A GEANT4-based detector simulation software BOOST [19] includes the geometric and material description of the BESIII detectors, the detector response, the digitization models, as well as the tracking of the detector running conditions and performances. Signal MC samples of $\psi(3770)$ and $\psi(4040)$ decay to baryonic final states containing 50 000 events for each channel at $\sqrt{s} = 3.773$ and 4.009 GeV are simulated by using the generator of KKMC [20], which includes initial state radiation (ISR). For the study of $\psi(3770)$ decay backgrounds, MC samples of $e^+e^- \rightarrow \gamma^{ISR}J/\psi$, $\gamma^{ISR}\psi(3686)$ equivalent to 1.5 times that of the data, and $e^+e^- \rightarrow \psi(3770) \rightarrow D\bar{D}$ and non- $D\bar{D}$ already measured experimentally [14] equivalent to 5.0 times that of the data are generated. For the study of $\psi(4040)$ decay backgrounds, about 1 fb^{-1} inclusive ISR MC samples (mainly $e^+e^- \rightarrow \gamma^{ISR}J/\psi$, $\gamma^{ISR}\psi(3686)$ and $\gamma^{ISR}\psi(3770)$) and $\psi(4040)$ direct decays (mainly open charm, hadronic and radiative transition production) equivalent to 2.1 times that of the data are generated. A scale factor f_{co} , which is used to normalize the continuum products to $\psi(3770)/\psi(4040)$ data, is determined by the integrated luminosities of the data sets corrected for an assumed $1/s$ dependence of the cross section. We also account for the small difference in efficiency between the $\psi(3770)/\psi(4040)$ data and continuum data. Therefore, MC samples of $e^+e^- \rightarrow$ baryonic final states containing 50 000 events for each mode at $\sqrt{s} = 3.773, 4.009, 3.542, 3.554, 3.561, 3.600$ and 3.650 GeV are also generated. The known decay modes of the charmonium states are produced by EVTGEN [21] with branching fractions being set to world average values [14] and the unknown ones by LUNDCHARM [22].

III. EVENT SELECTION

The analysis approach and selection criteria are as follows. Normal requirements are used to select charged particles reconstructed in the tracking system and photon candidates reconstructed in the electro-magnetic calorimeter (EMC). Charged tracks in BESIII are reconstructed from the main drift chamber (MDC) hits with good helix fits, which satisfy $|\cos\theta| < 0.93$, where θ is the polar angle with respect to e^+ direction. The charged tracks used in reconstructing Λ , Σ^+ , Σ^0 , Ξ^- and Ξ^0 decays are not required to satisfy a primary vertex requirement. Particle identification is used for each charged particle candidate. We use the combined energy loss in the drift chamber (dE/dx) and time-of-flight (TOF) information to compute the particle identification (PID) confidence levels ($CL_{\pi,K,p}$) for the hypotheses that the charged track is a π , K or p . We assign the track to be the π with the requirement of $CL_{\pi} > CL_K$, or to be the p with the requirement of $CL_p > 0.001$, $CL_p > CL_{\pi}$ and $CL_p > CL_K$. We require tracks of proton and anti-proton to have transverse momenta $p_{xy} > 300$ MeV/ c due to differences in the detection efficiencies between data and Monte Carlo simulation for low-momentum protons and anti-protons.

Electromagnetic showers are reconstructed from clusters of energy deposits in the EMC. Efficiency and energy resolution are improved by adding the energy deposits in nearby TOF counters. Good photon candidates are required to satisfy that a shower with an energy deposited in the barrel region ($|\cos\theta| < 0.8$) is at least 25 MeV, or at least 50 MeV in the end caps region ($0.86 < |\cos\theta| < 0.92$). To suppress showers generated by charged particles, the angle between the photon and the closest charged track is required to be greater than 10° . Requirements on the EMC cluster hit timing are used to suppress electronic noise and energy deposits unrelated to the event.

We identify intermediate states through the following decays: $\Lambda \rightarrow p\pi^-$, $\pi^0 \rightarrow \gamma\gamma$, $\eta \rightarrow \gamma\gamma$, $\Sigma^+ \rightarrow p\pi^0$ ($\pi^0 \rightarrow \gamma\gamma$), $\Sigma^0 \rightarrow \Lambda\gamma$ ($\Lambda \rightarrow p\pi^-$), $\Xi^- \rightarrow \Lambda\pi^-$ ($\Lambda \rightarrow p\pi^-$), $\Xi^0 \rightarrow \Lambda\pi^0$ ($\pi^0 \rightarrow \gamma\gamma$, $\Lambda \rightarrow p\pi^-$). For $\Lambda \rightarrow p\pi^-$, a vertex fit of p and π^- trajectories to a common vertex separated from the e^+e^- interaction point is made. To eliminate random $p\pi^-$ combinations, the secondary vertex fit algorithm is applied to impose the kinematic constraint between the production and decay vertex with the run-by-run averaged interaction point and the fitted p and π^- vertex information. For baryon pair modes ($\Sigma^+\bar{\Sigma}^0$, $\Xi^-\bar{\Xi}^+$, $\Xi^0\bar{\Xi}^0$), we only employ a vertex fit of p and π^- to reconstruct Λ . A loose requirement for the invariant mass of $p\pi^-$ to be in the range $|M(p\pi^-) - M(\Lambda)| < 40$ MeV/ c^2 is used for all the modes containing Λ in order to improve the efficiency, where $M(\Lambda)$ is the known mass of Λ [14]. For $\Xi^- \rightarrow \Lambda\pi^-$, a vertex fit of Λ and π^- to a common vertex is also made.

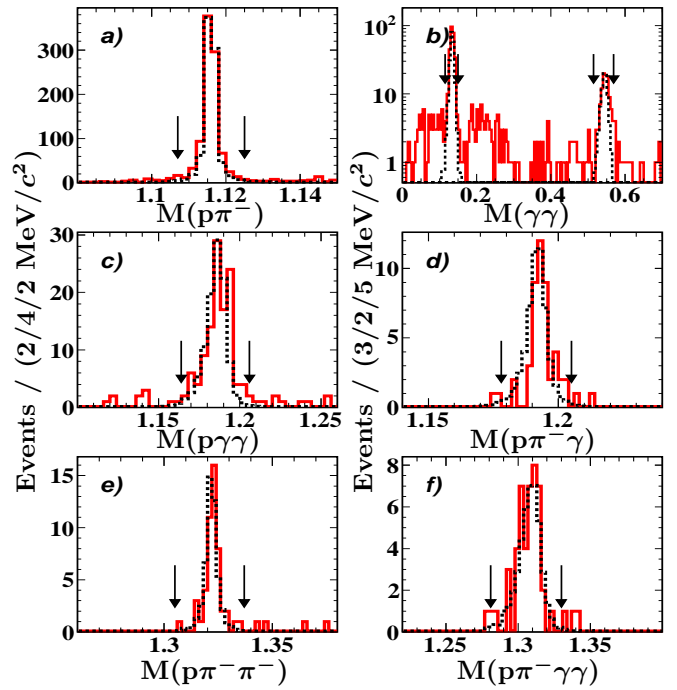


FIG. 1: Invariant mass distributions for intermediate states in units of GeV/ c^2 . Pairs of arrows indicate the signal region. Solid histogram: data at $\sqrt{s} = 3.773$ GeV, dashed histogram: signal MC, arbitrary normalization. (a) $\Lambda \rightarrow p\pi^-$, (b) $\pi^0 \rightarrow \gamma\gamma$ and $\eta \rightarrow \gamma\gamma$ with log scale, (c) $\Sigma^+ \rightarrow p\pi^0$ ($\pi^0 \rightarrow \gamma\gamma$), (d) $\Sigma^0 \rightarrow \Lambda\gamma$ ($\Lambda \rightarrow p\pi^-$), (e) $\Xi^- \rightarrow \Lambda\pi^-$ ($\Lambda \rightarrow p\pi^-$), and (f) $\Xi^0 \rightarrow \Lambda\pi^0$ ($\pi^0 \rightarrow \gamma\gamma$, $\Lambda \rightarrow p\pi^-$).

For each mode, the reconstructed events passing the above selection criteria are subjected to a four constraint (4-C) kinematic fit to make use of momentum and energy conservation between the initial state (e^+e^- beams) and the final states. The charged or neutral tracks comprising these events each have several combinations to pass through the four constraint kinematic fit, and only the combination with the smallest χ^2_{4-C} , the χ^2 of the 4-C kinematic fit, is retained for further study. We require $\chi^2_{4-C} < 60$ in order to suppress the backgrounds and improve the signal-to-background ratio.

For the final states with two π^0 s, because there exist several combinations for four γ s to form the two π^0 s, the candidate events with the minimum $R(\pi^0)$, where $R(\pi^0) = \sqrt{(M(\gamma\gamma)_1 - M(\pi^0))^2 + (M(\gamma\gamma)_2 - M(\pi^0))^2}$, are selected for further analysis. Here, $M(\pi^0)$ is the known mass of π^0 [14]. For the baryon pair modes $\Sigma^+\bar{\Sigma}^-$, $\Sigma^0\bar{\Sigma}^0$ and $\Xi^0\bar{\Xi}^0$, since they are formed by states of $p\bar{p}\pi^0\pi^0$, $\Lambda\bar{\Lambda}\gamma\gamma$ and $\Lambda\bar{\Lambda}\pi^0\pi^0$, there are also multiple solutions to make up the baryon pairs, and we select the minimum value of $R(j) = \sqrt{(M(i) - M(j))^2 + (M(i') - M(j))^2}$ as the optimized one, where i denotes $p\pi^0$, $\Lambda\gamma$ and $\Lambda\pi^0$, i' is $\bar{p}\pi^0$, $\bar{\Lambda}\gamma$ and $\bar{\Lambda}\pi^0$, j means Σ^+ , Σ^0 and Ξ^0 , $M(i)$ and $M(i')$ are the invariant mass of i and i' , $M(j)$ is the known mass of j [14].

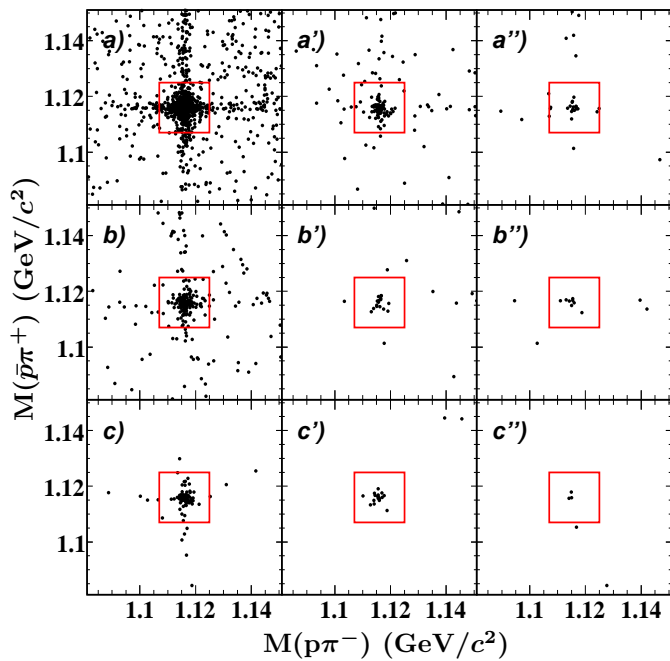


FIG. 2: Invariant mass of $p\pi^-$ versus $\bar{p}\pi^+$ distributions for $\Lambda\bar{\Lambda}\pi^+\pi^-$ [(a), (a') and (a'')], $\Lambda\bar{\Lambda}\pi^0$ [(b), (b') and (b'')], $\Lambda\bar{\Lambda}\eta$ [(c), (c') and (c'')]. The rectangle regions indicate signal regions. The figures on the left (middle, right) side: data at $\sqrt{s} = 3.773$ [4.009, continuum (3.543, 3.554, 3.561, 3.600 and 3.650)] GeV.

For every final state, the invariant mass distributions of the reconstructed intermediate states have the signal range determined from Monte Carlo studies: Λ ($1.107 \leq M(p\pi^-) \leq 1.124$ GeV/ c^2), π^0 ($115 \leq M(\gamma\gamma) \leq 150$ MeV/ c^2), η ($515 \leq M(\gamma\gamma) \leq 569$ MeV/ c^2), Σ^+ ($1.164 \leq M(p\gamma\gamma) \leq 1.206$ GeV/ c^2), Σ^0 ($1.178 \leq M(p\pi^-\gamma) \leq 1.205$ GeV/ c^2), Ξ^- ($1.305 \leq M(p\pi^-\pi^-) \leq 1.337$ GeV/ c^2), Ξ^0 ($1.281 \leq M(p\pi^-\gamma\gamma) \leq 1.330$ GeV/ c^2). For $\Xi^0\bar{\Xi}^0$, the selection of π^0 has a looser requirement of $110 \leq M(\gamma\gamma) \leq 150$ MeV/ c^2 due to the clean signal. With regard to any of the unstable particles, the signal range is about 3σ around the known mass of the particle, and the sideband range (not shown) is approximately from 5σ to 8σ at each side of the particle, where σ is the resolution determined by Monte Carlo simulation. In Fig. 1, the invariant mass distributions are shown for each reconstructed intermediate state, for which the events pass all the above selections.

For each mode studied, the signal selection region in the two dimensional scatter plot is determined by Monte Carlo simulation. In Figs. 2 and 3, the two dimensional scatter plots are shown for each mode. The rectangle regions are the signal regions. For final states of $\Lambda\bar{\Lambda}\pi^0$ and $\Lambda\bar{\Lambda}\eta$, the plots show the distributions by requiring π^0 and η to be in the signal range. To determine signal yields, the sideband events from π^0 and η must be removed. We first extract the number of events in one particle signal range with the requirement that the other

particle falls in its signal and sideband range, defined to be 'signal' and 'sideband', respectively, and then obtain the observed events N_{obs} after removing the normalized 'sideband' events from 'signal'.

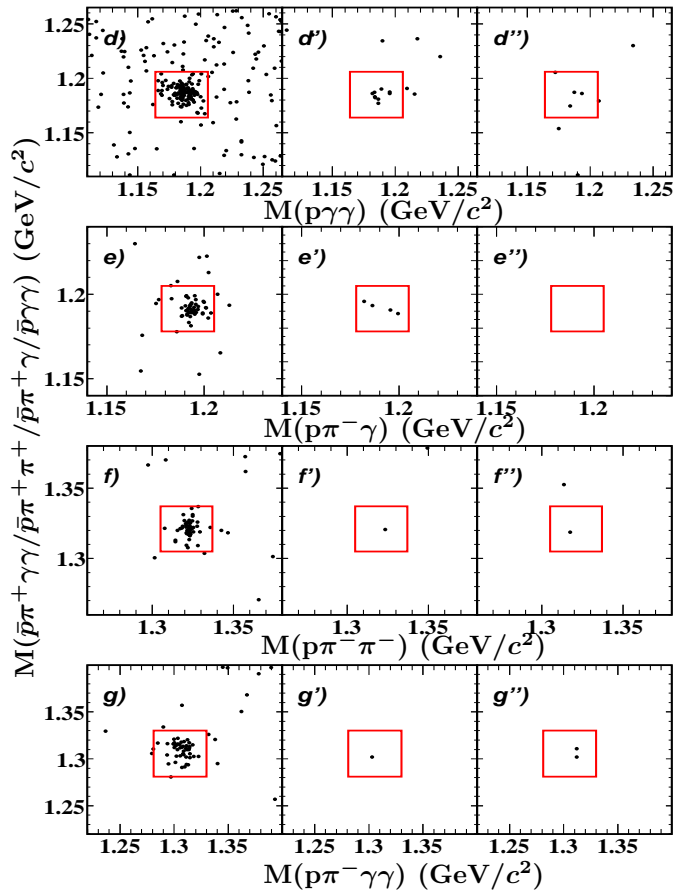


FIG. 3: Invariant mass of $p\gamma\gamma$, $p\pi^-\gamma$, $p\pi^-\pi^-$ or $p\pi^-\gamma\gamma$ versus $\bar{p}\gamma\gamma$, $\bar{p}\pi^+\pi^+$, $\bar{p}\pi^+\pi^+$ or $\bar{p}\pi^+\gamma\gamma$ distributions for $\Sigma^+\Sigma^-$ [(d), (d') and (d'')], $\Sigma^0\Sigma^0$ [(e), (e') and (e'')], $\Xi^-\Xi^+$ [(f), (f') and (f'')], $\Xi^0\bar{\Xi}^0$ [(g), (g') and (g'')]. The rectangle regions indicate signal regions. The figures on the left (middle, right) side: data at $\sqrt{s} = 3.773$ [4.009, continuum (3.543, 3.554, 3.561, 3.600 and 3.650)] GeV.

IV. BACKGROUND ESTIMATION

Our foremost observable is the background-subtracted number of the baryonic events inferred to be directly from $\psi(3770)$ and $\psi(4040)$ decays, $N_{\psi(3770)\rightarrow f}^S$ and $N_{\psi(4040)\rightarrow f}^S$. For the data taken at the center-of-mass energy of 3.773 GeV, the background contributions to the baryonic final states come from continuum production $e^+e^- \rightarrow q\bar{q} \rightarrow f$, $N_{q\bar{q}}^f(3.773)$, the initial state radiative returns to $\psi(3686)$ and J/ψ production $e^+e^- \rightarrow \gamma^{ISR}\psi(3686)$ (J/ψ) $\rightarrow f$, $N_{\gamma\psi(3686)}^f(3.773)$ ($N_{J/\psi}^f(3.773)$), and the misidentified $\psi(3770)$ direct de-

cays mainly containing $D\bar{D}$ production, $N_{D\bar{D}}^f(3.773)$. For the data taken at the center-of-mass energy of 4.009 GeV, the background contributions to the baryonic final states come from continuum production $e^+e^- \rightarrow q\bar{q} \rightarrow f$, $N_{q\bar{q}}^f(4.009)$, the initial state radiative returns to $\psi(3770)$, $\psi(3686)$ and J/ψ production $e^+e^- \rightarrow \gamma^{ISR}\psi(3770)$ ($\psi(3686)$, J/ψ) $\rightarrow f$, $N_{ISR}^f(4.009)$, and the misidentified $\psi(4040)$ direct decays containing open charm (DD), hadronic (hadrons) and radiative (gammaXYZ) production, $N_{DHG}^f(4.009)$.

Based on the Monte Carlo samples of $e^+e^- \rightarrow \gamma^{ISR}J/\psi$, $\gamma^{ISR}\psi(3686)$, and $e^+e^- \rightarrow \psi(3770) \rightarrow D\bar{D}$ generated at the center-of-mass energy 3.773 GeV, the backgrounds of $N_{\gamma\psi(3686)}^f(3.773)$, $N_{\gamma J/\psi}^f(3.773)$ and $N_{D\bar{D}}^f(3.773)$ were studied by employing the similar analysis strategy as described previously. Thus this part of background, $N_B^f(3.773)$, is given by

$$\begin{aligned} N_B^f(3.773) &= f_{\gamma\psi(3686)} \times N_{\gamma\psi(3686)}^f(3.773) \\ &+ f_{\gamma J/\psi} \times N_{\gamma J/\psi}^f(3.773) \\ &+ f_{D\bar{D}} \times N_{D\bar{D}}^f(3.773), \end{aligned} \quad (1)$$

where $f_{\gamma\psi(3686)} = f_{\gamma J/\psi} = 1/1.5$ and $f_{D\bar{D}} = 1/5.0$ are the scale factors for the Monte Carlo samples. The results of $N_B^f(3.773)$ are listed in Table I.

Using the Monte Carlo samples of $e^+e^- \rightarrow \gamma^{ISR}J/\psi$, $\gamma^{ISR}\psi(3686)$, $\gamma^{ISR}\psi(3770)$, and $e^+e^- \rightarrow \psi(4040) \rightarrow DD$, hadrons, gammaXYZ generated at the center-of-mass energy 4.009 GeV, the backgrounds of $N_{ISR}^f(4.009)$ and $N_{DHG}^f(4.009)$ are studied by employing the similar analysis strategy as described previously. Thus this part of background, $N_B^f(4.009)$, is given by

$$\begin{aligned} N_B^f(4.009) &= f_{ISR} \times N_{ISR}^f(4.009) \\ &+ f_{DHG} \times N_{DHG}^f(4.009) \end{aligned} \quad (2)$$

where $f_{ISR} = f_{DHG} = 1/2.1$ are the scale factors for the Monte Carlo samples. The results of $N_B^f(4.009)$ are listed in Table II.

To estimate the largest background at center-of-mass energies of 3.773 and 4.009 GeV, the continuum production $e^+e^- \rightarrow \gamma^* \rightarrow q\bar{q} \rightarrow f$, $N_{q\bar{q}}^f(3.773)$ and $N_{q\bar{q}}^f(4.009)$, the data taken at center-of-mass energies of 3.542, 3.554, 3.561, 3.600 and 3.650 GeV, which have small contaminations from the $\psi(3686)$ lower end intrinsic tail decays as well as of radiative returns to J/ψ decays, is used.

Hence $N_{q\bar{q}}^f(3.773/4.009)$ is obtained by

$$\begin{aligned} N_{q\bar{q}}^f(3.773/4.009) &= f_{co}^{3.773/4.009} \times N_{q\bar{q}}^f(3.650) \\ &= f_{co}^{3.773/4.009} \times [N_{obs}^f(3.650) \\ &\quad - N_B^f(3.650)] \\ &= f_{co}^{3.773/4.009} \times [N_{obs}^f(3.650) \\ &\quad - N_{\psi(3686)}^f(3.650) - N_{\gamma J/\psi}^f(3.650)], \end{aligned} \quad (3)$$

where $N_{obs}^f(3.650)$ is the observed number of baryonic final state events in the continuum data taken at center-of-mass energies of 3.542, 3.554, 3.561, 3.600 and 3.650 GeV, from which we scale the events from the first four energy points to the energy point of 3.650 GeV by considering the different efficiency and the assumed $1/s$ dependence of the cross section, $N_{\psi(3686)}^f(3.650)$ and $N_{\gamma J/\psi}^f(3.650)$ are the number of baryonic final state events from $\psi(3686)$ and J/ψ decays, respectively. $N_{\gamma J/\psi}^f(3.650)$ is obtained in the same way as previously described but at the center-of-mass energy of 3.650 GeV. $N_{\psi(3686)}^f(3.650)$ is given by $N_{\psi(3686)}^f(3.650) = \sigma_{\psi(3686)}^{3.650} \times \mathcal{L} \times \epsilon_{\psi(3686) \rightarrow f}^{3.650}$, where $\sigma_{\psi(3686)}^{3.650}$ is the cross section for $\psi(3686)$ production at the center-of-mass energy of 3.650 GeV [2], and $\epsilon_{\psi(3686) \rightarrow f}^{3.650}$ is the baryonic final state event selection efficiency of events from $\psi(3686) \rightarrow f$ at the center-of-mass energy of 3.650 GeV, determined by Monte Carlo simulation. The scaling factor, $f_{co}^{3.773/4.009}$, is mode dependent and determined by the integrated luminosities of the two data sets corrected for an assumed $1/s$ dependence of the cross section, and accounts for the small difference in efficiency between the $\psi(3770)/\psi(4040)$ data and continuum data. The uncertainty of $f_{co}^{3.773/4.009}$, about 2.0%-3.0%, arises from the uncertainties in relative luminosity and detection efficiencies at the two energy points. The results of $N_{obs}^f(3.650)$, $N_B^f(3.650)$ and $f_{co}^{3.773/4.009}$ are also listed in Table I and Table II.

V. RESULTS

We assume that there is no interference between continuum production and the $\psi(3770)/\psi(4040)$ resonance decay to the same baryonic final state. To obtain the number of baryonic final state events from $\psi(3770)/\psi(4040)$ direct decays, $N_{\psi(3770)/\psi(4040) \rightarrow f}^S$, we define $N_{\psi(3770)/\psi(4040) \rightarrow f}^S$ as

$$\begin{aligned} N_{\psi(3770)/\psi(4040) \rightarrow f}^S &= N_{obs}^f(3.773/4.009) \\ &\quad - N_B^f(3.773/4.009) \\ &\quad - N_{q\bar{q}}^f(3.773/4.009), \end{aligned} \quad (4)$$

where $N_{obs}^f(3.773/4.009)$ is the observed number of baryonic final state events in the $\psi(3770)/\psi(4040)$

TABLE I: For each mode f the following quantities are given: the number of observed events, $N_{obs}^f(3.773)$, and background events, $N_B^f(3.773)$, containing $N_{\gamma\psi(3686)}^f(3.773)$, $N_{\gamma J/\psi}^f(3.773)$ and $N_{D\bar{D}}^f(3.773)$ in $\psi(3770)$ data; the number of observed events, $N_{obs}^f(3.650)$, and background events, $N_B^f(3.650)$, containing $N_{\psi(3686)}^f(3.650)$ and $N_{\gamma J/\psi}^f(3.650)$ in continuum data; the scale factor $f_{co}^{3.773}$; the number of events attributable to $\psi(3770)$ decay, $N_{\psi(3770)\rightarrow f}^S$, computed according to Eq. (4); the upper limits on the number of events for $\psi(3770)$ baryonic decays including the systematic error (90% C.L.), $N_{\psi(3770)\rightarrow f}^{up}$; the detection efficiency ϵ ; the relative systematic error coming from the uncertainty in luminosity, intermediate state branching fractions, Monte Carlo statistics and the total number of $\psi(3770)$ decays, Δ_{sys} ; the branching fraction $\mathcal{B}_{\psi(3770)\rightarrow f}$; and the branching fraction upper limits for $\psi(3770)$ decays including the systematic errors (90% C.L.), \mathcal{B}^{up} .

Mode f	$N_{obs}^f(3.773)$	$N_B^f(3.773)$	$N_{obs}^f(3.650)$	$N_B^f(3.650)$	$f_{co}^{3.773}$	$N_{\psi(3770)\rightarrow f}^S$	$N_{\psi(3770)\rightarrow f}^{up}$	ϵ	Δ_{sys}	$\mathcal{B}_{\psi(3770)\rightarrow f}$ [$\times 10^{-4}$]	\mathcal{B}^{up} [$\times 10^{-4}$]
$\Lambda\bar{\Lambda}\pi^+\pi^-$	844.0 ± 33.6	5.2	$14.2^{+5.6}_{-4.2}$	0.1	45.27	$200.6^{+193.1}_{-255.7} \pm 42.0$	481.2	0.1321	8.0	$1.80^{+1.74}_{-2.30} \pm 0.40$	< 4.7
$\Lambda\bar{\Lambda}\pi^0$	124.9 ± 14.4	3.4	$7.1^{+5.0}_{-2.2}$	0.0	42.50	$-180.3^{+94.6}_{-213.0} \pm 16.2$	83.6	0.1694	8.0	$-1.28^{+0.67}_{-1.51} \pm 0.15$	< 0.7
$\Lambda\bar{\Lambda}\eta$	74.0 ± 9.5	0.9	$3.0^{+3.6}_{-1.6}$	0.0	44.76	$-61.2^{+72.2}_{-261.4} \pm 7.9$	87.7	0.1518	8.1	$-1.22^{+1.44}_{-3.21} \pm 0.19$	< 1.9
$\Sigma^+\Sigma^-$	100.5 ± 11.9	0.7	$3.3^{+4.3}_{-1.7}$	0.1	38.27	$-22.7^{+66.1}_{-165.0} \pm 5.1$	96.0	0.1975	8.0	$-0.21^{+0.63}_{-1.56} \pm 0.05$	< 1.0
$\Sigma^0\Sigma^0$	43.5 ± 6.7	0.0	$0.0^{+2.2}_{-0.0}$	0.0	38.69	$43.5^{+6.7}_{-85.4} \pm 5.8$	56.6	0.1752	8.0	$0.30^{+0.05}_{-0.58} \pm 0.05$	< 0.4
$\Xi^-\Xi^+$	48.5 ± 7.0	0.0	$0.5^{+2.8}_{-1.4}$	0.0	41.74	$27.6^{+58.9}_{-117.1} \pm 3.7$	119.7	0.1060	8.1	$0.31^{+0.66}_{-1.32} \pm 0.05$	< 1.5
$\Xi^0\Xi^0$	43.5 ± 6.6	1.3	$2.0^{+3.2}_{-1.2}$	0.0	40.13	$-38.1^{+48.6}_{-128.6} \pm 5.6$	60.7	0.0581	8.2	$-0.80^{+1.03}_{-2.72} \pm 0.14$	< 1.4

TABLE II: For each mode f the following quantities are given: the number of observed events, $N_{obs}^f(4.009)$, and background events, $N_B^f(4.009)$, containing $N_{ISR}^f(4.009)$, $N_{DHG}^f(4.009)$ in $\psi(4040)$ data; the number of observed events, $N_{obs}^f(3.650)$, and background events, $N_B^f(3.650)$, containing $N_{\psi(3686)}^f(3.650)$ and $N_{\gamma J/\psi}^f(3.650)$ in continuum data; the scale factor $f_{co}^{4.009}$; the number of events attributable to $\psi(4040)$ decay, $N_{\psi(4040)\rightarrow f}^S$, computed according to Eq. (4); the upper limits on the number of events for $\psi(4040)$ baryonic decays including the systematic error (90% C.L.), $N_{\psi(4040)\rightarrow f}^{up}$; the detection efficiency ϵ ; the relative systematic error coming from the uncertainty in luminosity, intermediate state branching fractions, Monte Carlo statistics and the number of $\psi(4040)$ decays, Δ_{sys} ; the branching fraction $\mathcal{B}_{\psi(4040)\rightarrow f}$; and the branching fraction upper limits for $\psi(4040)$ decays including the systematic errors (90% C.L.), \mathcal{B}^{up} .

Mode f	$N_{obs}^f(4.009)$	$N_B^f(4.009)$	$N_{obs}^f(3.650)$	$N_B^f(3.650)$	$f_{co}^{4.009}$	$N_{\psi(4040)\rightarrow f}^S$	$N_{\psi(4040)\rightarrow f}^{up}$	ϵ	Δ_{sys}	$\mathcal{B}_{\psi(4040)\rightarrow f}$ [$\times 10^{-4}$]	\mathcal{B}^{up} [$\times 10^{-4}$]
$\Lambda\bar{\Lambda}\pi^+\pi^-$	79.2 ± 10.0	20.0	$14.2^{+5.6}_{-4.2}$	0.1	7.69	$-49.2^{+33.8}_{-44.2} \pm 9.8$	35.6	0.1492	9.9	$-3.57^{+2.45}_{-3.21} \pm 0.79$	< 2.9
$\Lambda\bar{\Lambda}\pi^0$	$14.5^{+4.1}_{-4.3}$	0.5	$7.1^{+5.0}_{-2.2}$	0.0	6.80	$-34.3^{+15.5}_{-34.3} \pm 3.0$	12.6	0.1753	9.9	$-2.14^{+0.97}_{-2.14} \pm 0.28$	< 0.9
$\Lambda\bar{\Lambda}\eta$	$16.0^{+4.2}_{-4.3}$	3.6	$3.0^{+3.6}_{-1.6}$	0.0	7.38	$-9.8^{+12.5}_{-26.1} \pm 3.3$	16.2	0.1674	9.9	$-1.60^{+2.06}_{-4.43} \pm 0.57$	< 3.0
$\Sigma^+\Sigma^-$	$8.5^{+3.0}_{-3.2}$	0.2	$3.3^{+4.3}_{-1.7}$	0.1	4.92	$-7.5^{+8.9}_{-21.4} \pm 1.5$	11.0	0.1704	9.9	$-0.74^{+0.89}_{-2.14} \pm 0.17$	< 1.3
$\Sigma^0\Sigma^0$	$4.0^{+3.2}_{-1.9}$	0.0	$0.0^{+2.2}_{-0.0}$	0.0	5.03	$4.0^{+3.2}_{-11.2} \pm 0.5$	8.9	0.1537	9.9	$0.28^{+0.23}_{-0.79} \pm 0.04$	< 0.7
$\Xi^-\Xi^+$	$1.0^{+2.2}_{-0.8}$	0.0	$0.5^{+2.8}_{-1.4}$	0.0	5.61	$-1.8^{+8.2}_{-15.7} \pm 0.3$	12.5	0.0941	9.9	$-0.21^{+0.94}_{-1.81} \pm 0.04$	< 1.6
$\Xi^0\Xi^0$	$1.0^{+2.2}_{-0.8}$	0.0	$2.0^{+3.2}_{-1.2}$	0.0	5.36	$-9.7^{+6.8}_{-17.2} \pm 1.3$	7.0	0.0490	10.0	$-2.22^{+1.55}_{-3.93} \pm 0.37$	< 1.8

data taken at the center-of-mass energy of 3.773/4.009 GeV. Since no statistically significant extra signal is observed, 90% C.L. upper limits on the number of events for $\psi(3770)/\psi(4040)$ baryonic decays are computed with systematic errors included for each mode, $N_{\psi(3770)/\psi(4040)\rightarrow f}^{up}$, by assuming that they follow a Gaussian distribution and considering only physical (positive) values. The relative systematic errors related to $N_{\psi(3770)/\psi(4040)\rightarrow f}^S$ include the independent and common systematic errors. The independent systematic errors depend on energy points and consist of uncertainty in background subtraction (0.0%-20.2%) and uncertainty in invariant mass spectrum fit (0.0%-5.1%). The common systematic errors do not depend on the energy point and include the uncertainty in invariant mass requirement for unstable particles (0.8%-3.4%) and also the detector performance related quantities: charged particle tracking (1.0% per track), photon selection (1.0% per

photon), $\pi/p/\bar{p}$ identification (1.0%/1.0%/2.0%), vertex and secondary vertex fit (1.0% each) and kinematic fit (1.0%-2.0%). Some of the modes have tiny component resonant submodes, however, the efficiencies do not differ by much. Monte Carlo samples are generated with a phase space model, and the difference of the efficiencies with and without intermediate states is taken as the systematic error (0.3%). Another systematic error for baryon pairs comes from the angular distribution, which is described by $1 + \alpha \cos^2\theta$, with θ being the polar angle. Monte Carlo samples are generated for $\alpha = 0$ and $\alpha = 1$, and the difference of efficiency between $\alpha = 0$ and $\alpha = 1$ is taken as the systematic error (9.2%-10.9%). The results of $N_{obs}^f(3.773/4.009)$, $N_{\psi(3770)/\psi(4040)\rightarrow f}^S$ and $N_{\psi(3770)/\psi(4040)\rightarrow f}^{up}$ are also shown in Tables I and II.

The number of baryonic final state events from $\psi(3770)/\psi(4040)$ decays, $N_{\psi(3770)/\psi(4040)\rightarrow f}^S$ is corrected

by the detection efficiency, ϵ and the related branching fractions for the intermediate state decays, B_f , and normalized to the total number of the $\psi(3770)/\psi(4040)$ decays to obtain the branching fraction.

$$\mathcal{B}_{\psi(3770)/\psi(4040)\rightarrow f} = \frac{N_{\psi(3770)/\psi(4040)\rightarrow f}^S}{\epsilon \times B_f \times N_{\psi(3770)/\psi(4040)}}, \quad (5)$$

The upper limit on the branching fraction can be obtained by

$$\mathcal{B}^{up} = \frac{N_{\psi(3770)/\psi(4040)\rightarrow f}^{up}}{\epsilon \times B_f \times N_{\psi(3770)/\psi(4040)} \times (1 - \Delta_{sys})}, \quad (6)$$

where the detection efficiency for $\psi(3770)/\psi(4040)$ baryonic decays, ϵ is estimated by using the Monte Carlo simulation of the BESIII detector based on the KKMC [20] and BesEvtGen [21] generators. The detection efficiencies in Tables I and II do not include the branching fractions for intermediate state decays. B_f is the branching fraction [14] for the intermediate state decays for each mode. $N_{\psi(3770)/\psi(4040)}$ is the number of $\psi(3770)/\psi(4040)$ decays and is determined by $N_{\psi(3770)/\psi(4040)} = \sigma_{\psi(3770)/\psi(4040)}^{Born-level} \times \mathcal{L}_{\psi(3770)/\psi(4040)} \times (1 + \delta)_{ISR}$, where $\sigma_{\psi(3770)/\psi(4040)}^{Born-level} = (9.93 \pm 0.77)/(6.2 \pm 0.6)$ nb is the Born-level cross section of $\psi(3770)/\psi(4040)$ at $\sqrt{s} = 3.773$ and 4.009 GeV obtained by the relativistic Breit-Wigner formula with the $\psi(3770)$ and $\psi(4040)$ resonance parameters [14]; $\mathcal{L}_{\psi(3770)/\psi(4040)}$ is the integrated luminosity for $\psi(3770)/\psi(4040)$ data and $(1 + \delta)_{ISR} = 0.718/0.757$ is the radiative correction factor, obtained from the KKMC [20] generator with the $\psi(3770)$ and $\psi(4040)$ resonance parameters [14] input. Δ_{sys} is the relative systematic error only involving the uncertainty in the integrated luminosity (1.1%), the intermediate state branching fractions (0.8%-1.2%), the Monte Carlo statistics (0.9%-2.0%) and a common uncertainty of 7.8%/9.7% due to the number of $\psi(3770)/\psi(4040)$ decays arising from the uncertainty in $\psi(3770)/\psi(4040)$ resonance parameters. We give the branching fractions $\mathcal{B}_{\psi(3770)/\psi(4040)\rightarrow f}$ and the upper limits on branching fractions \mathcal{B}^{up} of $\psi(3770)/\psi(4040)$ baryonic decays for each mode in Tables I and II. Since the available continuum data is limited, the dominant error on each of the seven branching fractions is from the continuum subtraction.

VI. SUMMARY

In summary, using 2.9 fb⁻¹ of data taken at $\sqrt{s} = 3.773$ GeV, 482 pb⁻¹ of data taken at $\sqrt{s} = 4.009$

GeV, 23 pb⁻¹ of data taken at $\sqrt{s} = 3.542, 3.554, 3.561$ and 3.600 GeV and 44 pb⁻¹ of data taken at $\sqrt{s} = 3.650$ GeV collected with the BESIII detector at the BEPCII collider, searches for seven baryonic decays of $\psi(3770)$ and $\psi(4040)$ are presented; most are the first searches. The upper limits on the branching fractions for $\psi(3770)$ and $\psi(4040)$ baryonic decays are set at the 90% C.L.. The sum of the seven branching fractions are $(-1.11_{-5.46}^{+2.72} \pm 0.72) \times 10^{-4}$ and $(-1.02_{-0.76}^{+0.39} \pm 0.15) \times 10^{-3}$, and the corresponding upper limits at the 90% C.L. are 4.0×10^{-4} and 3.1×10^{-4} for the seven baryonic decays of $\psi(3770)$ and $\psi(4040)$, respectively. Although this study, together with previous studies on searching for exclusive non- $D\bar{D}$, provide useful information for understanding the nature of $\psi(3770)$, the large non- $D\bar{D}$ component still remains a puzzle. A fine energy scan over $\psi(3770)$ and $\psi(4040)$ resonances would be very helpful for obtaining the lineshape of exclusive non- $D\bar{D}$ processes, and help determine whether the processes exist or not.

VII. ACKNOWLEDGEMENT

The BESIII collaboration thanks the staff of BEPCII and the computing center for their strong support. This work is supported in part by the Ministry of Science and Technology of China under Contract No. 2009CB825200, 2009CB825204; National Natural Science Foundation of China (NSFC) under Contracts Nos. 10625524, 10821063, 10825524, 10835001, 10935007, 11125525, 11235011; Joint Funds of the National Natural Science Foundation of China under Contracts Nos. 11079008, 11179007; the Chinese Academy of Sciences (CAS) Large-Scale Scientific Facility Program; CAS under Contracts Nos. KJCX2-YW-N29, KJCX2-YW-N45; 100 Talents Program of CAS; German Research Foundation DFG under Contract No. Collaborative Research Center CRC-1044; Istituto Nazionale di Fisica Nucleare, Italy; Ministry of Development of Turkey under Contract No. DPT2006K-120470; U. S. Department of Energy under Contracts Nos. DE-FG02-04ER41291, DE-FG02-05ER41374, DE-FG02-94ER40823; U.S. National Science Foundation; University of Groningen (RuG) and the Helmholtzzentrum fuer Schwerionenforschung GmbH (GSI), Darmstadt; WCU Program of National Research Foundation of Korea under Contract No. R32-2008-000-10155-0

[1] M. Ablikim *et al.*, (BES Collaboration), Phys. Lett. B **659**, 74 (2008).

[2] M. Ablikim *et al.*, (BES Collaboration), Phys. Rev. D

- 76**, 122002 (2007).
- [3] M. Ablikim *et al.*, (BES Collaboration), Phys. Rev. Lett. **97**, 121801 (2006).
- [4] M. Ablikim *et al.*, (BES Collaboration), Phys. Lett. B **641**, 145 (2006).
- [5] D. Besson *et al.*, (CLEO Collaboration), Phys. Rev. Lett. **104**, 159901 (2010).
- [6] D. Besson *et al.*, (CLEO Collaboration), Phys. Rev. Lett. **96**, 092002 (2006).
- [7] E. Eichten *et al.*, Phys. Rev. Lett. **34**, 369 (1975).
- [8] E. Eichten *et al.*, Phys. Rev. D **21**, 203 (1980).
- [9] J. Z. Bai *et al.*, (BES Collaboration), Phys. Lett. B **605**, 63 (2005).
- [10] N. E. Adam *et al.*, (CLEO Collaboration), Phys. Rev. Lett. **96**, 082004 (2006).
- [11] T. E. Coan *et al.*, (CLEO Collaboration), Phys. Rev. Lett. **96**, 182002 (2006).
- [12] R. A. Briere *et al.*, (CLEO Collaboration), Phys. Rev. D **74**, 031106 (2006).
- [13] G. S. Adams *et al.*, (CLEO Collaboration), Phys. Rev. D **73**, 012002 (2006).
- [14] J. Beringer *et al.*, (Particle Data Group), Phys. Rev. D **86**, 010001 (2012).
- [15] M. Ablikim *et al.*, (BESIII Collaboration), Phys. Rev. D **86**, 071101 (2012).
- [16] M. Ablikim *et al.*, (BESIII Collaboration), Nucl. Instrum. Meth. A **614**, 345 (2010).
- [17] J. Z. Bai *et al.*, (BES Collaboration), Nucl. Instrum. Meth. A **344**, 319 (1994); Nucl. Instrum. Meth. A **458**, 627 (2001).
- [18] D. M. Asner *et al.*, Int. J. Mod. Phys. A **24**, 499 (2009).
- [19] Z. Y. Deng *et al.*, Chinese Phys. C **30**, 371 (2006).
- [20] S. Jadach, B. F. L. Ward and Z. Was, Comput. Phys. Commun. **130**, 260 (2000); S. Jadach, B. F. L. Ward and Z. Was, Phys. Rev. D **63**, 113009 (2001).
- [21] R. G. Ping *et al.*, Chinese Phys. C **32**, 599 (2008).
- [22] J. C. Chen *et al.*, Phys. Rev. D **62**, 034003 (2000).